Further insights into platinum carbonyl Chini clusters

Further Insights into Platinum Carbonyl Chini Clusters

Beatrice Berti[a], Marco Bortoluzzi[b], Alessandro Ceriotti[c], Cristiana Cesari[a], Cristina Femoni[a], Maria Carmela Iapalucci[a], Stefano Zacchini[a,*]

[a] Dipartimento di Chimica Industriale "Toso Montanari", Università di Bologna, Viale Risorgimento 4 - 40136 Bologna, Italy. E-mail: stefano.zacchini@unibo.it

[b] Dipartimento di Scienze Molecolari e Nanosistemi, Ca' Foscari University of Venice, Via Torino 155 – 30175 Mestre (Ve), Italy.

[c] Dipartimento di Chimica, Università degli Studi di Milano, via Golgi 19, 20133 Milano, Italy.

Abstract: The oxidation of $[Ph_3P(CH_2)_{12}PPh_3][Pt_{15}(CO)_{30}]$ with CF_3COOH in THF afforded $[Ph_3P(CH_2)_{12}PPh_3][Pt_{18}(CO)_{36}]$ as a precipitate which was re-crystallized from dmf/iso-propanol. This salt self-assembles in the solid state adopting an unprecedented morphology which consists of infinite chains of $[Pt_9(CO)_{18}]^-$ units. The solid state structure of $[Ph_3P(CH_2)_{12}PPh_3][Pt_{18}(CO)_{36}]$ may be viewed as a snapshot in which $[Pt_9(CO)_{18}]^-$ units are approaching and ready to exchange outer $Pt_3(CO)_6$ fragments. The reactions of Chini clusters with isonitriles proceed via redox-fragmentation, at difference with those involving phosphines that may occur both via non-redox substitution and redox fragmentation, depending on the experimental conditions. Thus, the reaction of $[Pt_6(CO)_{12}]^{2-}$ with CNXyl afforded $Pt_5(CNXyl)_{10}$, whereas $Pt_9(CNXyl)_{13}(CO)$ was obtained from the reaction of $[Pt_{15}(CO)_{30}]^{2-}$ with CNXyl. These two new neutral clusters have been structurally characterized as their $Pt_5(CNXyl)_{10}$·2toluene and $Pt_9(CNXyl)_{13}(CO)$·solv solvates. DFT studies on the CO exchange of $[Pt_6(CO)_{12}]^{2-}$ suggest an associative interchange mechanism, which may be extended also to larger Chini clusters and the initial steps of their reactions with other soft nucleophiles.

Dedicated to Maurizio Peruzzini on occasion of his 65th birthday.

Keywords: Cluster compounds; Carbonyl ligands; Platinum; Self-assembly; Nanoscience

1. Introduction

Platinum carbonyl cluster of the general formula $[Pt_{3n}(CO)_{6n}]^{2-}$ (n = 1-10), usually referred as Chini clusters, represent a milestone in inorganic chemistry and cluster science [1]. They are conveniently prepared by reductive carbonylation of Pt-salts under very mild conditions and isolated with miscellaneous organic or organometallic cations [1-4]. Their molecular structures consist of stacks of $Pt_3(CO)_3(\mu\text{-}CO)_3$ units arranged in a trigonal prismatic fashion along a *pseudo*-C_3 axis [1-6]. All Chini clusters with *n* ranging from 2 to 8 have been structurally characterized by means of single-crystal X-ray diffraction (SC-XRD). They display shorter inter-triangular and longer intra-triangular Pt-Pt bonds. Moreover, clusters with $n \geq 5$ often self-assemble in the solid state, affording infinite conductive molecular Pt-wires [7,8]. The tendency of larger Chini cluster to self-assemble into infinite molecular wires has been exploited for the fabrication of Pt-wires and conductive nanowires [9], as also evidenced by TEM and STM analyses [10,11].

Along the years, Chini clusters have been exploited in catalysis as molecular entities or as precursors of nanostructured catalytic materials [2,3,12-20]. Recently, Chini clusters have been also employed for the generation and stabilization of small platinum clusters inside a metal-organic framework [21]. The resulting materials have been employed in the catalytic hydrogenation of 1-hexene and electrocatalytic oxygen reduction reaction.

Chini clusters display a very rich and fascinating chemistry. $[Pt_{3n}(CO)_{6n}]^{2-}$ clusters may be reversibly oxidized to higher nuclearity $[Pt_{3(n+1)}(CO)_{6(n+1)}]^{2-}$ species [1,8]. Moreover, CO ligands may be replaced by soft nucleophiles resulting in heteroleptic Chini type-clusters [22-24]. Thermal decomposition of Chini clusters under mild conditions affords globular platinum molecular nanoclusters (platinum browns) which may be viewed as atomically precise CO-protected ultrasmall Pt-nanoparticles [25]. Finally, the reactions of $[Pt_{3n}(CO)_{6n}]^{2-}$ cluster with metal salts can be exploited for the preparation of bimetallic clusters [26-29].

The topic of Chini clusters has been recently reviewed [2,3]. Herein, we have collected some further results on the chemistry of Chini clusters. In particular, a new self-assembly morphology of $[Pt_{3n}(CO)_{6n}]^{2-}$ clusters is reported, together with additional studies on the reactions of Chini clusters with soft nucleophiles. The ability of Chini clusters to exchange CO ligands has been computationally investigated by means of DFT calculations on the $[Pt_6(CO)_{12}]^{2-}$ cluster.

2.Results and Discussion

2.1 Self-assembly of Chini clusters

Self-assembly of $[Pt_{3n}(CO)_{6n}]^{2-}$ clusters in the solid state was previously discussed and herein some further examples are added [7,8]. The nature of the resulting structures depends on the sizes of the

cluster anion and the cation employed (Figure 1). Indeed, it has been shown that lower nuclearity clusters ($n \leq 4$) always result in ionic 0-D packings, with the anions and cations separated by normal Van der Waals contacts. Conversely, larger clusters ($n \geq 5$) may form infinite chains in the solid state, which can be discontinuous, semi-continuous or continuous, depending on the reciprocal nature of the cluster anion and cation. In discontinuous chains, the cluster anions retain their molecular identity, having the outer $Pt_3(CO)_6$ units of consecutive cluster anions separated by distances slightly above the sum of the Van der Waals radii. In the opposite side, continuous chains comprise infinite stacks of $Pt_3(CO)_6$ units at bonding distances and, therefore, the molecular identity of the single anion is lost. Semi-continuous chains represent an intermediate structure where a $Pt_3(CO)_6$ unit is shared by two contiguous $[Pt_{3(n-1)}(CO)_{6(n-1)}]^{2-}$ anions and displays Pt-Pt interactions intermediate between those of continuous and discontinuous chains. Moreover, semi-continuous chains can be symmetric or asymmetric: in symmetric semi-continuous chains the shared $Pt_3(CO)_6$ unit shows similar distances to the two contiguous $[Pt_{3(n-1)}(CO)_{6(n-1)}]^{2-}$ fragments, whereas the two distances are different in the case of asymmetric semi-continuous chains.

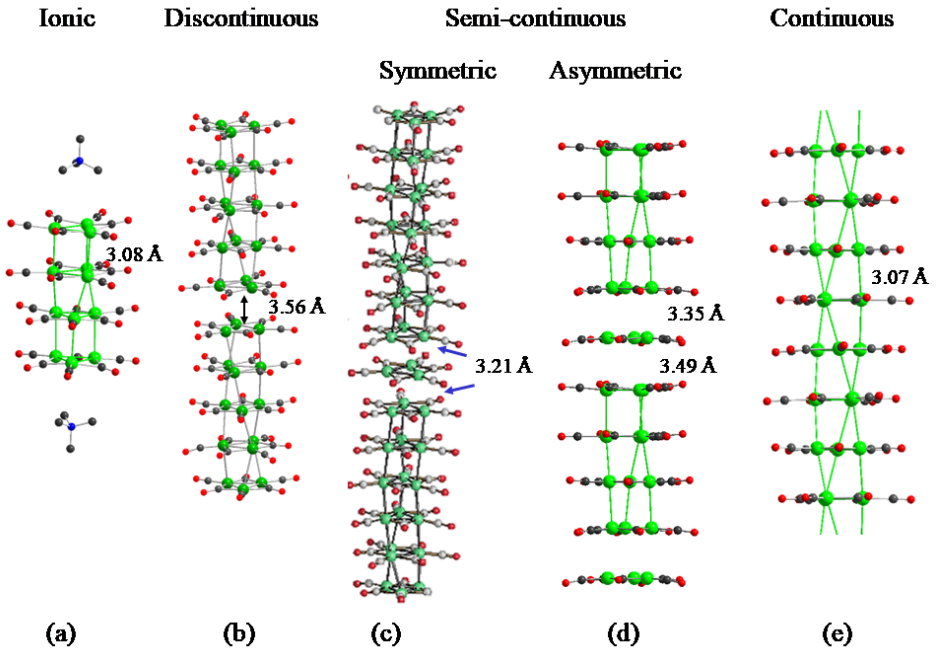

Fig. 1. Typical arrangements of $[Pt_{3n}(CO)_{6n}]^{2-}$ (n = 4–8) clusters in (a) ionic, (b) discontinuous, (c) symmetric semi-continuous, (d) asymmetric semi-continuous and (e) continuous chains, as found in their solid state structures with miscellaneous cations [7,8].

In addition, these chains of clusters can be further organized into 1-D, 2-D or 3-D packings. Within 1-D structures, the chains of clusters are aligned along a single direction (parallel chains), whereas they are arranged along two different directions (layered packing) in 2-D packings or three non-coplanar directions in the case of 3-D structures [7,8].

So far, all the $[Pt_{3n}(CO)_{6n}]^{2-}$ anions with n = 2-8 have been structurally characterized in the presence of $[NR_4]^+$ (R = Me, Et, Bu), $[PPh_4]^+$, $[AsPh_4]^+$, $[Ru(tpy)_2]^{2+}$ (tpy = 2,2':6',2''-terpyridine), $[Ru(bpy)_3]^{2+}$ (bpy = 2,2'-bipyridyl) and $[Ni(macro)]^{2+}$ (macro = 5,7,7,12,14,14-hexamethyl-1,4,8,11-tetraaza-4,11-cyclotetradecadiene) cations [1,4,7,8]. Most of these cations are almost spherical and it has been shown that their diameter somehow influences the crystal packing of Chini clusters. So, it was of interest to study the packing and self-assembly of the same clusters in the presence of cations with different shapes. In particular, elongated cations such as $[Ph_3P(CH_2)_{12}PPh_3]^{2+}$, $[Ph_3P(CH_2)_6PPh_3]^{2+}$ and $[DAMS]^+$ (DAMS = 2-(4-dimethylaminostyryl)-1-methylpyridinium) have been considered.

The general synthetic procedure consisted in preparing the $Na_2[Pt_{3n}(CO)_{6n}]$ salts in CH_3OH solution as previously described in the literature [1,2,7,8], followed by cation metathesis using solutions of $[Ph_3P(CH_2)_6PPh_3][Br]_2$ and $[Ph_3P(CH_2)_{12}PPh_3][Br]_2$ in H_2O, or [DAMS]I in CH_3OH (Scheme 1). In the presence of these cations, Chini clusters immediately precipitated and the solids were recovered by filtration, dried under reduced pressure and extracted with organic solvents (see Experimental for further details). In this way, crystals of $[Ph_3P(CH_2)_6PPh_3][Pt_{15}(CO)_{30}]$ and $[DAMS]_2[Pt_9(CO)_{18}]\cdot$dmf were obtained. Conversely, $[Ph_3P(CH_2)_{12}PPh_3][Pt_{18}(CO)_{36}]$ was obtained in two steps. First, $[Ph_3P(CH_2)_{12}PPh_3][Pt_{15}(CO)_{30}]$ was prepared as described above. Then, this salts was dissolved in THF and oxidized with CF_3COOH *via* the H^+/H_2 redox couple. $[Ph_3P(CH_2)_{12}PPh_3][Pt_{18}(CO)_{36}]$ precipitated out from the reaction mixture and was, eventually, dissolved in dmf and crystallized by slow diffusion of isopropanol. The new salts $[Ph_3P(CH_2)_{12}PPh_3][Pt_{18}(CO)_{36}]$, $[Ph_3P(CH_2)_6PPh_3][Pt_{15}(CO)_{30}]$ and $[DAMS]_2[Pt_9(CO)_{18}]\cdot$dmf have been structurally characterized by SC-XRD. The structures of the molecular cations and anions present in these salts are reported in Figures 2 and 3, whereas the main bond distances are summarized in Table 1.

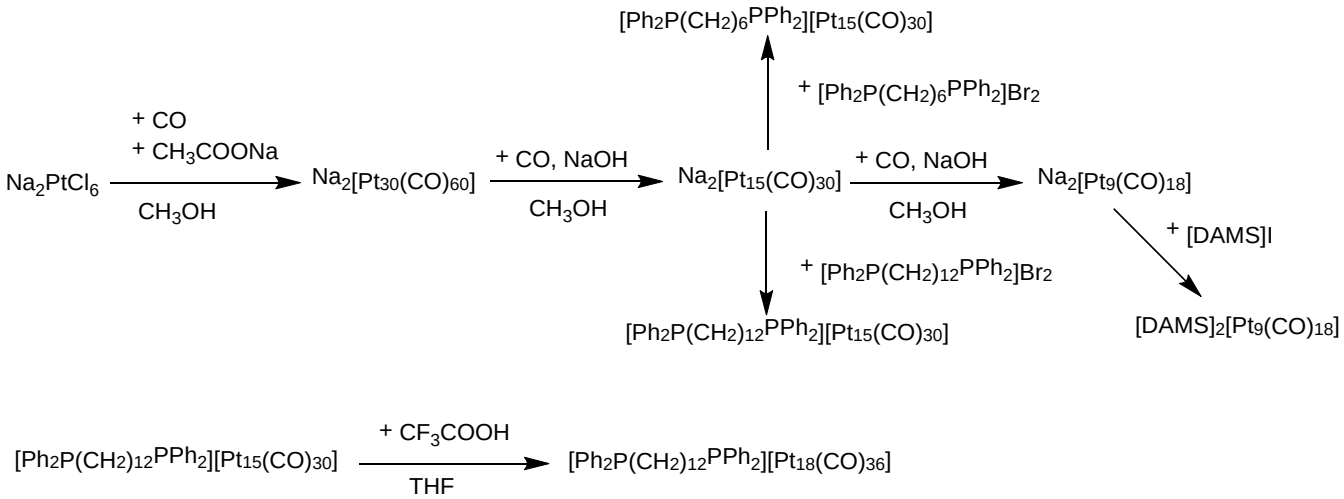

Scheme 1. Synthesis of $[Ph_3P(CH_2)_{12}PPh_3][Pt_{18}(CO)_{36}]$, $[Ph_3P(CH_2)_6PPh_3][Pt_{15}(CO)_{30}]$ and $[DAMS]_2[Pt_9(CO)_{18}]\cdot dmf$.

The crystal packing of the $[Ph_3P(CH_2)_6PPh_3][Pt_{15}(CO)_{30}]$ and $[DAMS]_2[Pt_9(CO)_{18}]\cdot dmf$ salts are typically ionic without any stacking of molecular clusters (0-D packing). This is not surprising for $[DAMS]_2[Pt_9(CO)_{18}]\cdot dmf$, since stacking phenomena are not observed for Chini clusters with $n \leq 4$. Conversely, in the case of $[Pt_{15}(CO)_{30}]^{2-}$ anions, the crystal packing is usually affected by the cation. Thus, $[Ru(bpy)_3][Pt_{15}(CO)_{30}]\cdot 3CH_3COCH_3$ contains asymmetric semi-continuous chains of clusters anions, whereas $[Ru(tpy)_2][Pt_{15}(CO)_{30}]\cdot 3DMF$ and $[NEt_4]_2[Pt_{15}(CO)_{30}]$ display discontinuous chains of clusters [7,8]. Isolated ions (0-D packing) are, conversely, observed in the case of $[AsPh_4]_2[Pt_{15}(CO)_{30}]$ [1] and the herein reported $[Ph_3P(CH_2)_6PPh_3][Pt_{15}(CO)_{30}]$.

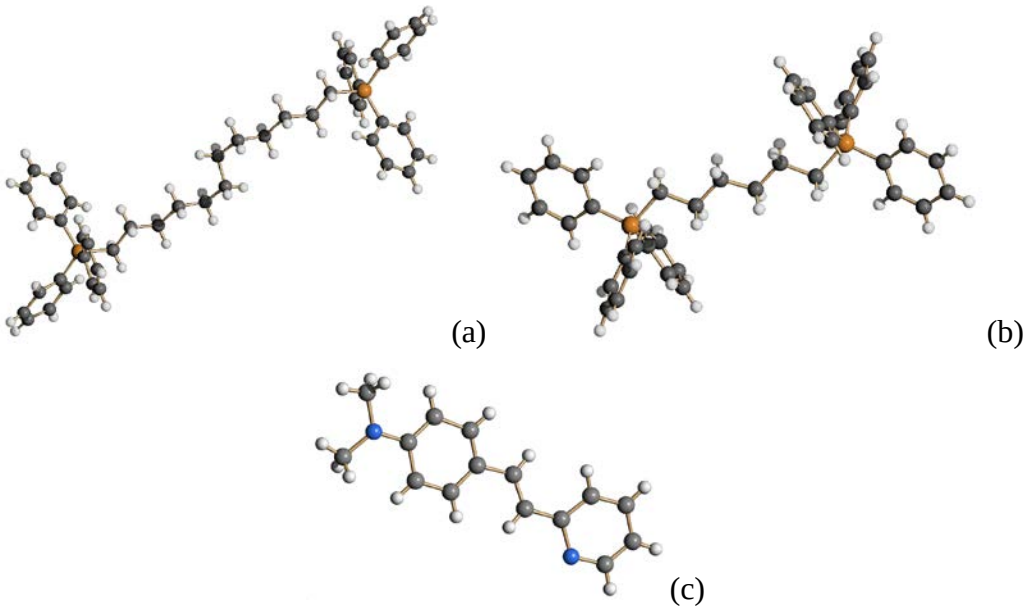

Fig. 2. Molecular structures of the cations: (a) $[Ph_3P(CH_2)_{12}PPh_3]^{2+}$, (b) $[Ph_3P(CH_2)_6PPh_3]^{2+}$, and (c) $[DAMS]^+$ (orange, P; blue, N; grey, C; white, H).

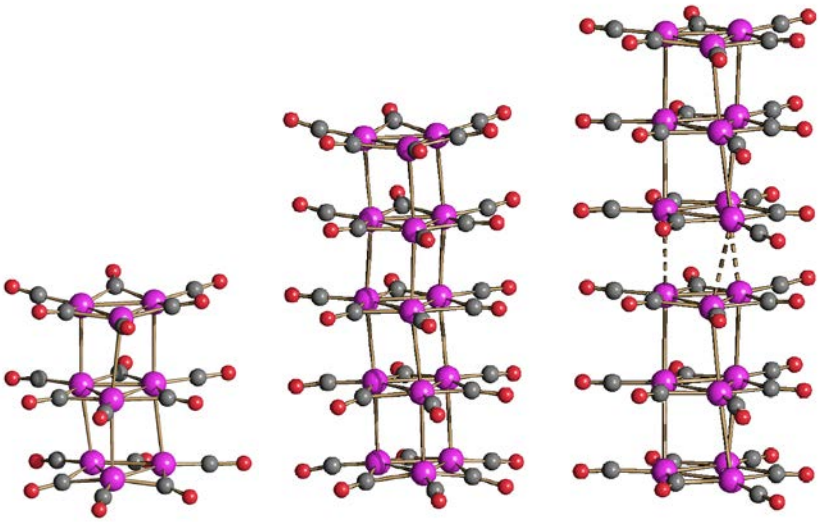

(a) (b) (c)

Fig. 3. Molecular structures of the anions: (a) $[Pt_9(CO)_{18}]^{2-}$ as found in $[DAMS]_2[Pt_9(CO)_{18}]\cdot dmf$, (b) $[Pt_{15}(CO)_{30}]^{2-}$ as found in $[Ph_3P(CH_2)_6PPh_3][Pt_{15}(CO)_{30}]$, and (c) $[Pt_{18}(CO)_{36}]^{2-}$ as found in $[Ph_3P(CH_2)_{12}PPh_3][Pt_{18}(CO)_{36}]$ (purple, Pt; red, O; grey, C). Pt-Pt bonds longer than 3.2 Å have been drawn as fragmented lines.

Table 1

Main bond distances (Å) for $[Pt_9(CO)_{18}]^{2-}$ as found in $[DAMS]_2[Pt_9(CO)_{18}]\cdot dmf$, $[Pt_{15}(CO)_{30}]^{2-}$ as found in $[Ph_3P(CH_2)_6PPh_3][Pt_{15}(CO)_{30}]$, and $[Pt_{18}(CO)_{36}]^{2-}$ as found in $[Ph_3P(CH_2)_{12}PPh_3][Pt_{18}(CO)_{36}]$

	Pt-Pt intra-triangular	**Pt-Pt inter-triangular**
$\mathbf{[Pt_9(CO)_{18}]^{2-}}$	2.653(2)-2.668(2)	3.0200(19)-3.044(2)
$\mathbf{[Pt_{15}(CO)_{30}]^{2-}}$	2.649(2)-2.6703(19)	2.9972(14)-3.0783(18)
$\mathbf{[Pt_{18}(CO)_{36}]^{2-}}$	2.6599(17)-2.6787(16)	3.1025(19)-3.327(4)

More interestingly, the arrangement of the $[Pt_{18}(CO)_{36}]^{2-}$ anions within the $[Ph_3P(CH_2)_{12}PPh_3][Pt_{18}(CO)_{36}]$ salt is completely unprecedented (Figure 4). Indeed, it contains infinite chains of $[Pt_9(CO)_{18}]^{-}$ units, which can be clearly distinguished because the inter-triangular Pt-Pt distances within each unit [3.1025(19)-3.1819(19) Å] are significantly shorter than the Pt-Pt distances between two

consecutive $[Pt_9(CO)_{18}]^-$ units [3.245(2)-3.327(4) Å]. The former distances are comparable to the normal Pt-Pt inter-triangular bonding contacts found in molecular Chini clusters, whereas the latter contacts are in the limiting region between weakly-bonding and non-bonding. For comparison, intra-triangular Pt-Pt contacts are in the narrow range 2.66-2.68 Å [1,4,7,8]. Within each $[Pt_9(CO)_{18}]^-$ unit, the distances between the centroids of the three Pt_3-triangules are 3.10 and 3.12 Å, whereas the distance between the centroids of the Pt_3-triangules of two consecutive $[Pt_9(CO)_{18}]^-$ units is 3.22 Å. This gap is typical of semi-continuous chains of Chini clusters. Nonetheless, in semi-continuous chains a single $Pt_3(CO)_6$ fragment is shared between two consecutive $[Pt_{3(n-1)}(CO)_{6(n-1)}]^{2-}$ units. Conversely, in the present case there are three consecutive $Pt_3(CO)_6$ fragments at normal bonding distances forming a $[Pt_9(CO)_{18}]^-$ unit, then a gap, then a second $[Pt_9(CO)_{18}]^-$ unit and so on. As a result, the molecular identity of each $[Pt_{18}(CO)_{36}]^{2-}$ anion is lost. These infinite chains of $[Pt_9(CO)_{18}]^-$ units are all parallel resulting in a 1-D packing of anions (Figure 5).

The resistivity of $[Ph_3P(CH_2)_{12}PPh_3][Pt_{18}(CO)_{36}]$ measured as pressed pellets is 8.5×10^5 Ω cm, *ca*. one order of magnitude greater than the values usually found for solids containing semi-continuous stacking of Chini clusters [1.5-6.5 × 10^4 Ω cm] [8]. This may be due to a partial confinement of the electrons within the $[Pt_9(CO)_{18}]^-$ units, without any Peierls deformation [6] in the 1-D packing of anions even at low T (100 K).

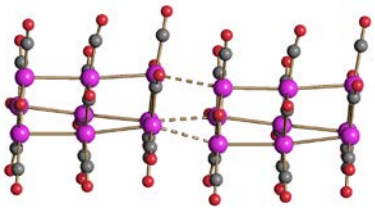

(a)

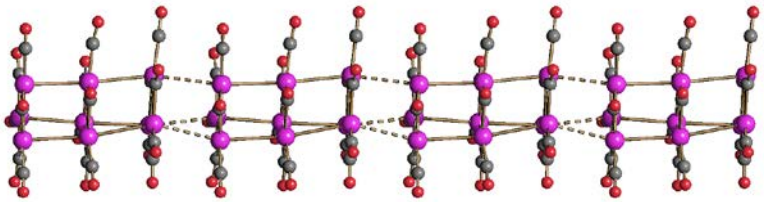

(b)

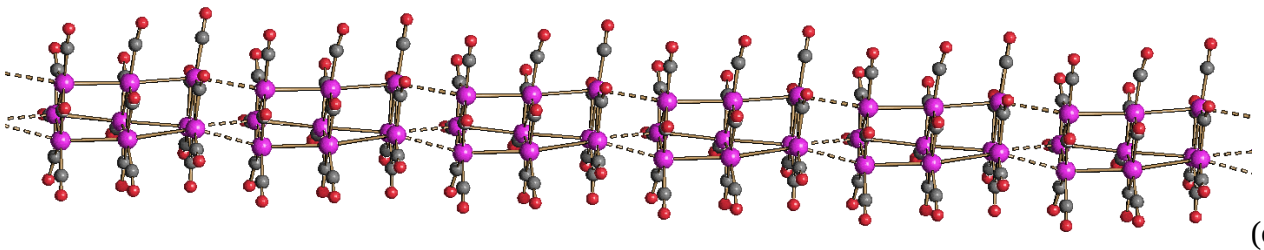

(c)

Fig. 4. Stacking of the $[Pt_{18}(CO)_{36}]^{2-}$ anions in $[Ph_3P(CH_2)_{12}PPh_3][Pt_{18}(CO)_{36}]$: (a) a single anion, (b) two anions, and (c) three anions (purple, Pt; red, O; grey, C). Pt-Pt bonds longer than 3.2 Å have been drawn as fragmented lines.

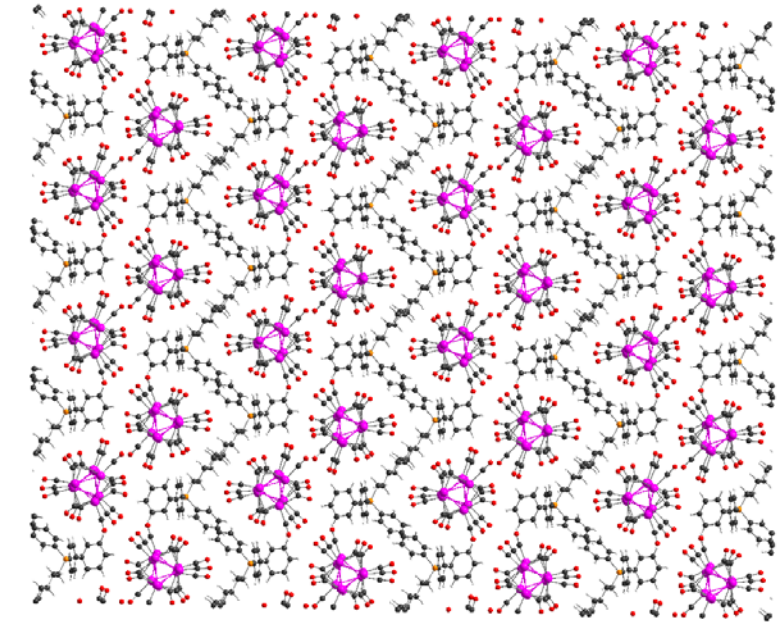

(a)

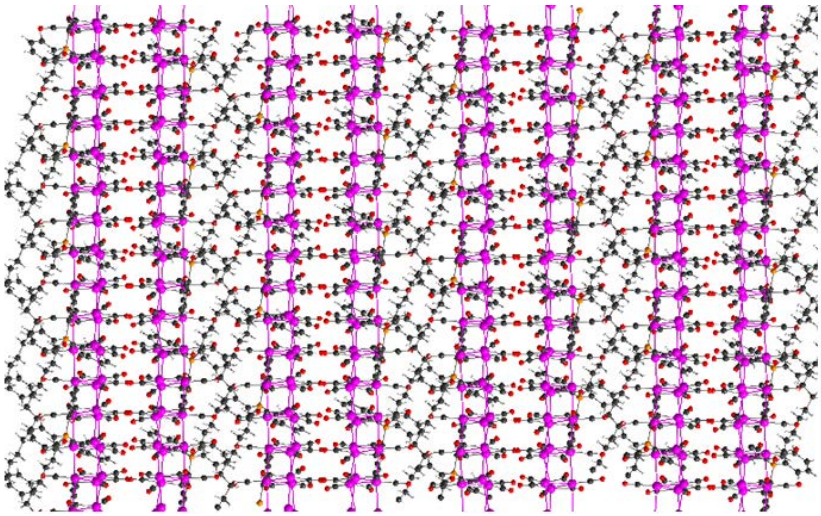

(b)

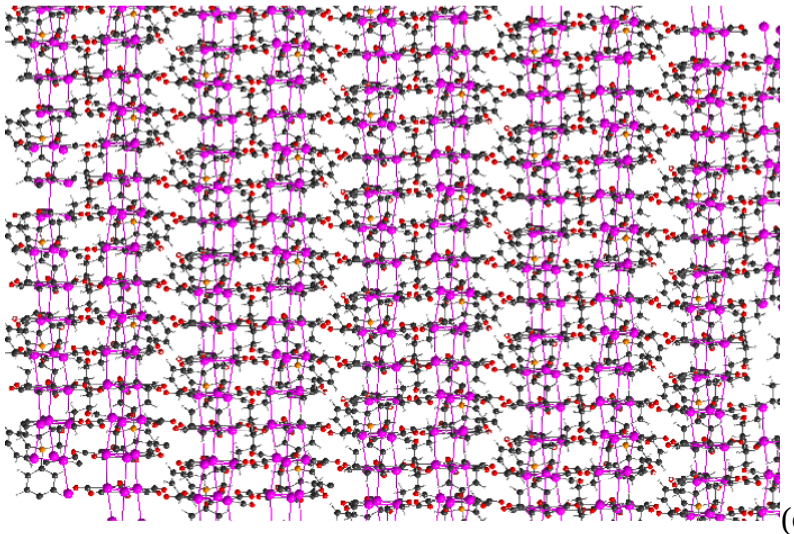
(c)

Fig. 5. Crystal packing of $[Ph_3P(CH_2)_{12}PPh_3][Pt_{18}(CO)_{36}]$: (a) view along the a-axis, (b) view along the v-axis, and (c) view along the c-axis, (purple, Pt; red, O; grey, C).

The assignment of a mono-anionic charge to the $[Pt_9(CO)_{18}]^{-}$ repeating unit of these polymeric chains is based on the fact that within the asymmetric unit of the unit cell there is a $Pt_9(CO)_{18}$ fragment and half of a $[Ph_3P(CH_2)_{12}PPh_3]^{2+}$ cation. $[Pt_{3n}(CO)_{6n}]^{-}$ mono-anions have been supposed to be involved in the oxidation of Chini clusters [30]. Indeed, it is well known that the oxidation of $[Pt_{3n}(CO)_{6n}]^{2-}$ affords higher nuclearity $[Pt_{3(n+1)}(CO)_{6(n+1)}]^{2-}$ clusters [1,2]. The mechanism is not well understood, but it is likely to involve mono-anionic species and exchange of triangles between Chini clusters. Thus, the solid state structure of $[Ph_3P(CH_2)_{12}PPh_3][Pt_{18}(CO)_{36}]$ may be viewed as a snapshot in which $[Pt_9(CO)_{18}]^{-}$ units are approaching and ready to exchange outer $Pt_3(CO)_6$ fragments.

2.2 Reactions with soft nucleophiles: non-oxidative addition vs. redox-fragmentation

The reaction of $[Pt_{3n}(CO)_{6n}]^{2-}$ clusters with phosphines ligands (L = PPh_3, PTA, $Ph_2PCH_2PPh_2$, dppe, $CH_2{=}C(PPh_2)_2$, *o*-$C_6H_4(PPh_2)_2$, *R*-$Ph_2PCH(Me)CH_2PPh_2$, $Fe(C_5H_4PPh_2)_2$, $Ph_2P(CH_2)_4PPh_2$, dppa; PTA = 1,3,5,triaza-7-phosphaadamantane; dppe = $Ph_2PCH_2CH_2PPh_2$; dppa = $Ph_2PC{\equiv}CPPh_2$) may afford $[Pt_{3n}(CO)_{6n-x}(L)_x]^{2-}$ heteroleptic Chini clusters *via* non-redox substitution, or lower nuclearity $[Pt_{3(n-1)}(CO)_{6(n-1)}]^{2-}$ homoleptic Chini clusters together with neutral Pt-L-CO complexes *via* redox-fragmentation [22-24]. The output of the reaction strongly depends on the stoichiometry, the nature of the phosphine ligand and the nuclearity of the cluster. Often a competition between

non-redox substitution and redox-fragmentation is observed. For instance, the reactions of $[Pt_{3n}(CO)_{6n}]^{2-}$ (n = 2-4) with dppe afford substitution products such as $[Pt_6(CO)_{10}(dppe)]^{2-}$, $[Pt_9(CO)_{16}(dppe)]^{2-}$ and $[Pt_{12}(CO)_{20}(dppe)_2]^{2-}$, as well as neutral species such as $Pt_6(CO)_6(dppe)_3$, $Pt_4(CO)_4(dppe)_2$, and $Pt(dppe)_2$. Redox-fragmentation is favoured by an excess of dppe. Indeed, performing the same reactions with a large excess of dppe, a new species displaying a unique ν_{CO} band at 1913 cm^{-1} was observed and isolated by selective extraction with toluene. Then, the new compound was crystallized from CH_2Cl_2/n-pentane and characterized by SC-XRD, disclosing the $Pt_2(dppe)_3(CO)_2 \cdot 2CH_2Cl_2$ solvate neutral complex. The molecular structure of $Pt_2(dppe)_3(CO)_2$ (Figure 6) is very similar to that previously reported for $Pt_2\{(CF_3CF_2)_2PCH_2CH_2P(CF_2CF_3)_2\}_3(CO)_2$ [31]. It consists of two Pt(0) centres tetrahedrally coordinated to one CO and three P-atoms. Two dppe units act as chelating ligands, one per Pt centre, whereas the third dppe ligand is bridging the two Pt-atoms. The coordination geometry and bonding parameters around each Pt-centre are very similar to that found in $Pt_2\{(CF_3CF_2)_2PCH_2CH_2P(CF_2CF_3)_2\}_3(CO)_2$ [31], $Pt_2(dppa)_3(CO)_2$ [23] and $Pt(PPh_3)_3(CO)$ [32].

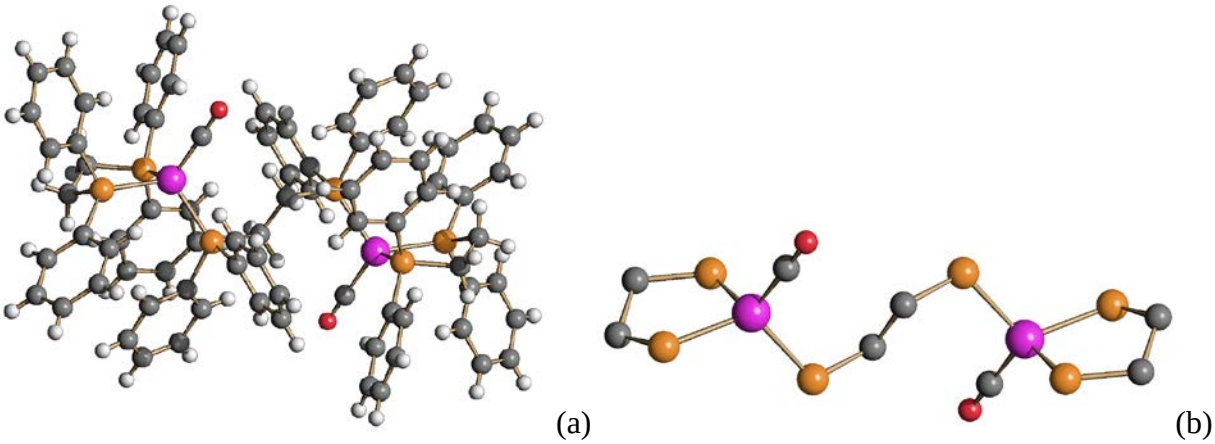

(a) (b)

Fig. 6. Molecular structure of $Pt_2(dppe)_3(CO)_2$: (a) complete view, and (b) simplified representation where H atoms and Ph-groups have been omitted (purple, Pt; orange, P; red, O; grey, C). Main bond distances: Pt-P 2.300(2)-2.3225(19) Å; Pt-C 1.894(8) Å; C-O 1.131(10) Å.

Chini clusters undergo to a rapid isotopic $^{12}CO/^{13}CO$ exchange when exposed to ^{13}CO even at pressures below 1 atm [33]. At the same time, Chini clusters are stable under N_2 and also under high *vacuum*, both in the solid state and in solution. This suggests that $^{12}CO/^{13}CO$ exchange as well as the reactions with phosphine ligands proceed *via* an associative mechanism. Indeed, if the mechanism was dissociative, Chini clusters should lose CO and decompose under *vacuum*. Thus,

species such as $[Pt_{3n}(^{12}CO)_{6n}(L)]^{2-}$ (L = ^{13}CO, phosphine or another soft nucleophile) might be involved in these reactions as intermediates or transition states.

The CO exchange was computationally investigated by means of DFT calculations on the $[Pt_6(CO)_{12}]^{2-}$ cluster. The addition of a further CO molecule afforded the $[Pt_6(CO)_{13}]^{2-}$ anion depicted in Figure 7 as intermediate (**INT**). Only one of the two Pt_3 triangles is noticeably affected by the addition of the new CO ligand, that interacts with Pt with linear coordination mode. The computed Pt-C bond lengths for the $[Pt(CO)_2]$ fragment are between 1.933 and 1.960 Å, slightly longer than those calculated for the terminal CO ligands in $[Pt_6(CO)_{12}]^{2-}$, in the 1.882 – 1.903 Å range. Starting from $[Pt_6(CO)_{13}]^{2-}$, the dissociation of one CO from the $[Pt(CO)_2]$ fragment was followed by means of coordinate driving calculations. As observable in Figure 7, the elongation of the Pt-C bond by 0.20 – 0.25 Å leads to a maximum in the energy profile. The corresponding structure is indicated as **TS** in Figure 7. The energy separation between **INT** and **TS** is small, about 1.6 kcal mol^{-1}, and the global structure of the molecule appears scarcely affected by the elongation, the RMSD being 0.698 Å. The similarity between **INT** and **TS** could explain why attempts with other approaches to find the transition state geometry for the reaction failed, affording **INT** as final result. It is worth noting that the elongation of one Pt-C bond in $[Pt(CO)_2]$ caused the shortening by 0.06 Å of the second one moving from **INT** to **TS**. Further elongation of the Pt-C bond caused the progressive reduction of the energy of the system, and for sufficient Pt---CO distances the structure is analogous to that obtained for $[Pt_6(CO)_{12}]^{2-}$ and free CO (**R**, Figure 7). The energy separation between **R** and **TS** is about 15.6 kcal mol^{-1}, suggesting that the process does not have strong kinetic barriers. The entropy contribution to the energy barrier estimated from calculations on separated $[Pt_6(CO)_{12}]^{2-}$, $[Pt_6(CO)_{13}]^{2-}$ and CO is around 9.1 kcal mol^{-1}. On considering the energy profile shown in Figure 7, the CO exchange can be considered as an associative interchange. Similar considerations might be applied to reactions with other soft nucleophiles.

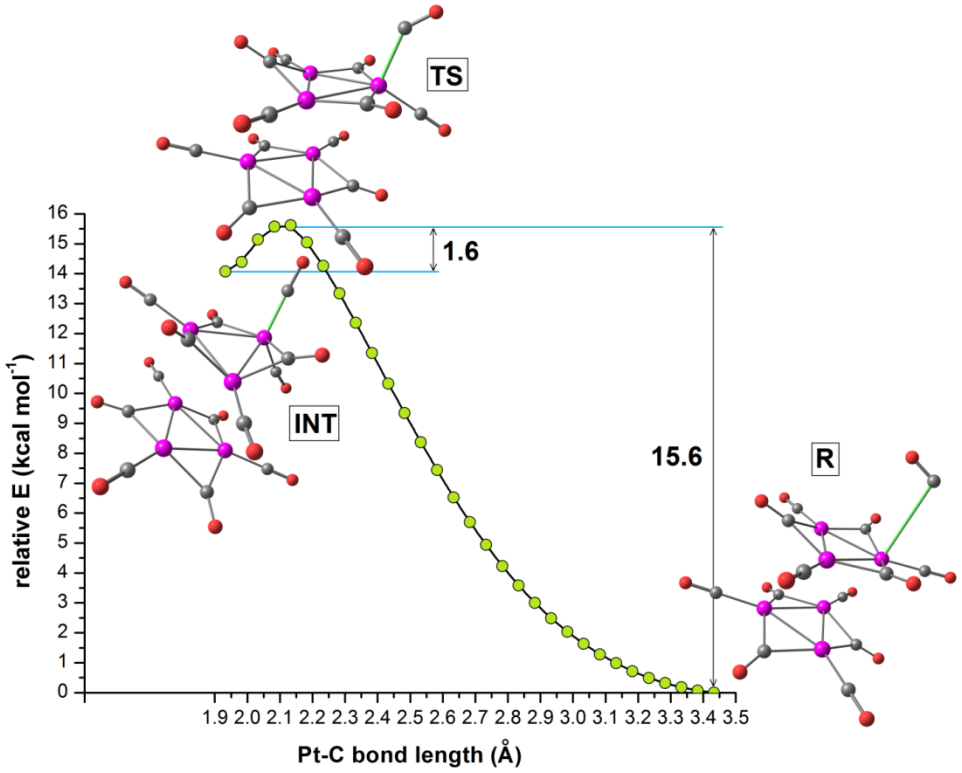

Fig. 7. Relative energy profile for the coordinate driving calculation of the dissociation of one carbonyl ligand from $[Pt_6(CO)_{13}]^{2-}$ (**INT**) (ωB97X/def2-SVP calculations). The elongated Pt-C bond is highlighted in green. DFT-optimized structures of **INT**, **TS** and **R** (purple, Pt; red, O; grey, C).

In the attempt to trap in the solid state a species of the type $[Pt_{3n}(CO)_{6n}(L)]^{2-}$, two different approaches have been used. First, $[NEt_4]_2[Pt_9(CO)_{18}]$ has been crystallized from a solution of pyridine by slow diffusion of isopropanol. The aim was to obtain a solid state structure where the pyridine molecule approached a Pt atom of the Chini cluster with its N-donor atom. As a result, crystals of $[NEt_4]_2[Pt_9(CO)_{18}]\cdot$py were obtained, but the pyridine molecule was not interacting with the cluster.

The second approach consisted in the reaction of $[Pt_{12}(CO)_{24}]^{2-}$ with two equivalents of PPh_2py, resulting in the substitution product $[Pt_{12}(CO)_{22}(PPh_2py)_2]^{2-}$ (Figure 8). In this case the aim was to force an interaction between the N-atom of the bidentate PPh_2py ligand and the cluster. Also this approach was not successful, since the crystals of $[NEt_4]_2[Pt_{12}(CO)_{22}(PPh_2py)_2]$ were isomorphous and isostructural with $[NEt_4]_2[Pt_{12}(CO)_{22}(PPh_3)_2]$ [22b].

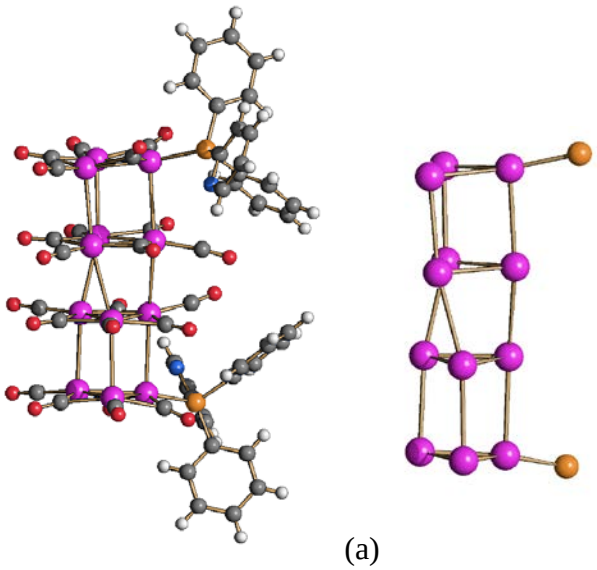

(a) (b)

Fig. 8. Molecular structure of (a) $[Pt_{12}(CO)_{22}(PPh_2py)_2]^{2-}$ and (b) its $Pt_{12}P_2$ skeleton (purple, Pt; orange, P; red, O; grey, C; blue, N; white, H). Main bond distances: Pt-Pt intra-triangular 2.6505(15)-2.6681(17) Å; Pt-Pt inter-triangular 2.9919(16)-3.173(2) Å; Pt-P 2.265(7) Å.

The reactions of Chini clusters have been, then, extended to other soft nucleophiles, and in particular isonitriles [34]. At differences with phosphines, all the reactions studied using isonitriles proceeded *via* redox fragmentation and not non-redox substitution (Scheme 2). Thus, the reaction of $[Pt_6(CO)_{12}]^{2-}$ with CNXyl afforded $Pt_5(CNXyl)_{10}$, whereas $Pt_9(CNXyl)_{13}(CO)$ was obtained from the reaction of $[Pt_{15}(CO)_{30}]^{2-}$ with CNXyl. These two new neutral clusters have been structurally characterized as their $Pt_5(CNXyl)_{10}$·2toluene and $Pt_9(CNXyl)_{13}(CO)$·solv solvates.

$$[Pt_6(CO)_{12}]^{2-} \xrightarrow[CH_3CN]{+\ CNXyl} Pt_5(CNXyl)_{10}$$

$$[Pt_{15}(CO)_{30}]^{2-} \xrightarrow[acetone]{+\ CNXyl} Pt_9(CNXyl)_{13}(CO)$$

Scheme 2. Synthesis of $Pt_5(CNXyl)_{10}$ and $Pt_9(CNXyl)_{13}(CO)$.

It must be remarked that Chini clusters are stable in CH_3CN under inert atmosphere, suggesting that they do not react with nitriles. The different reactivity of $[Pt_{3n}(CO)_{6n}]^{2-}$ with nitriles

and isonitriles can be explained on the basis of their different π-acidity. Nitriles are very poor π-acid and, therefore, they cannot replace CO in anionic Chini clusters. Isonitriles are better π-acid than nitriles (but poorer than CO) and, if used in excess, they react with Chini clusters.

The molecular structure of $Pt_5(CNXyl)_{10}$ consists of an edge-bridged Pt_5 tetrahedron bonded to five μ-CNXyl and five terminal CNXyl ligands (Figure 9). The metal core and stereochemistry of the ligands is the same found in related $Pt_5(CO)_6(PR_3)$ (R = Ph, Cy, $CH_2C(O)Ph$) [35] and $Pt_5(CO)_7(IMes)_3$(IMes =) clusters [26]. Conversely, $Pt_5(CNXyl)_8(P(Ph)_2CH_2C(O)Ph)_2$ displays the same Pt_5 core but, probably because of steric problems, only three CNXyl ligands are edge bridging, whereas all the remaining ligands are in terminal positions. $Pt_5(CNXyl)_{10}$ possesses 70 cluster valence electrons (CVE) as previously found in related species. On the basis of the Effective Atomic Number (EAN) rule an edge bridged tetrahedron should have 74 CVE [36]. Thus, all these Pt_5L_{10} species are electron poor, as often found in Pt-clusters.

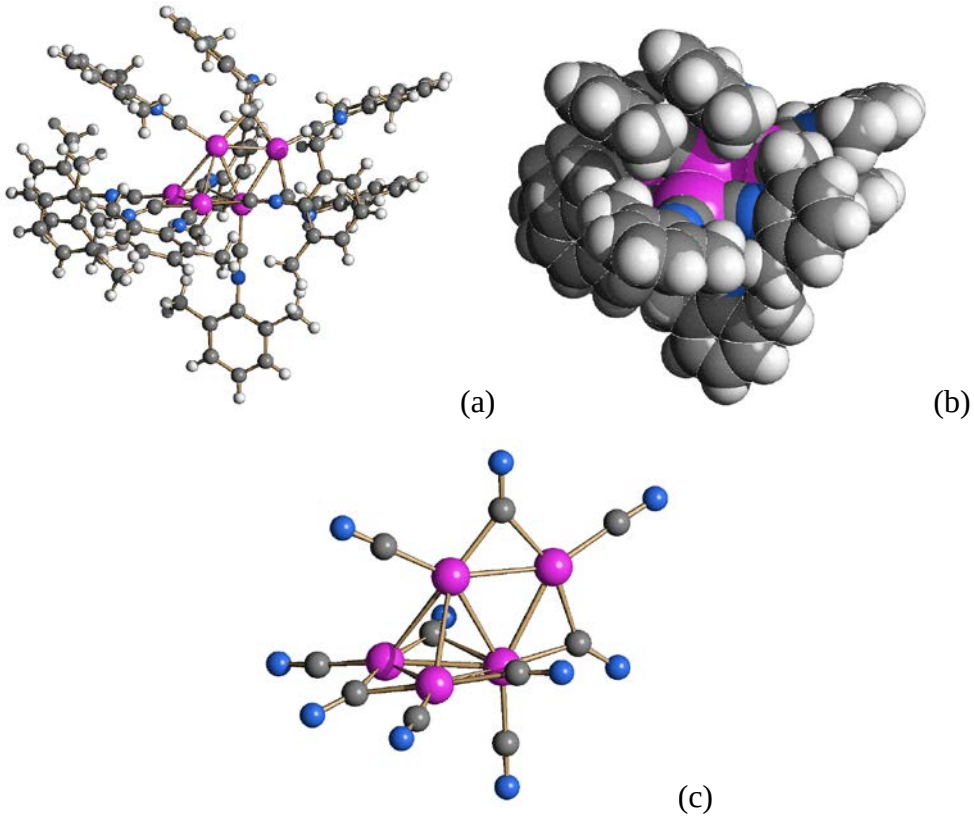

Fig. 9. (a) Molecular structure of $Pt_5(CNXyl)_{10}$, (b) space filling model, and (c) a simplified view of the metal skeleton and stereochemistry of the ligands (purple, Pt; orange, P; blue, N; grey, C; white, H). Main bond distances: Pt-Pt 2.6561(6)-2.8513(7) Å; Pt-$C_{terminal}$ 1.913(14)-1.929(13) Å; Pt-

$C_{bridging}$ 2.000(12)-2.548(13) Å; $C_{terminal}$-N 1.142(16)-1.156(17) Å; $C_{bridging}$-N 1.148(16)-1.230(16) Å.

The molecular structure of $Pt_9(CNXyl)_{13}(CO)$ is unprecedented (Figure 10). Its metal core consists of a Pt_7 pentagonal bipyramid (PBP) with two further Pt-atoms capping two non-adjacent triangular faces which share a common vertex. A few examples of clusters displaying a M_7-PBP core have been reported, but these were capped on adjacent triangular faces or on M-M edges [37,38]. Alternatively, $Pt_9(CNXyl)_{13}(CO)$ may be considered as based on the removal of three vertices from a $Pt_{12}(\mu_{12}$-Pt) centred icosahedron. The cluster contains one edge bridging CO, eight terminal CNXyl ligands, four μ-CNXyl and one μ_3-η^2-CNXyl. The latter ligand may be viewed as a four-electron donor, whereas all the other are two-electron donor ligands. Thus, $Pt_9(CNXyl)_{13}(CO)$ possesses 118 CVE as expected for a nine-vertex cluster displaying 22 M-M bonds. The μ_3-η^2 coordination of CNR ligands is rather uncommon and relevant examples include $[Pd_6(CNXyl)_{12}]^+$ [39], $Ru_3(CO)_6(PhPCH_2PPh_2)(CNCy)_3$ [40], $Pt_7(CNXyl)_{12}$ [41], $Ni_4(CN^tBu)_7$[42], $Os_6(CO)_{18}$(CN-*p*-$MeC_6H_4)_2$ [43], $Ni_4(CN^tBu)_5\{P(NSiMe_3)(N(SiMe_3)_2\}_2$ [44].

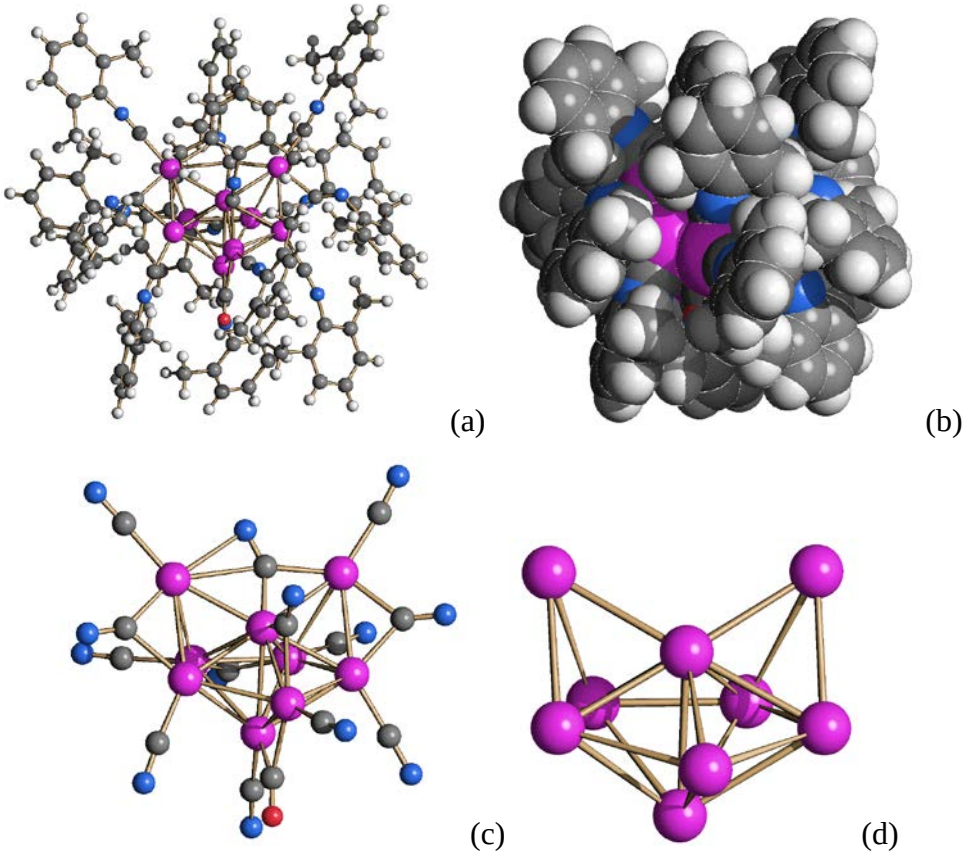

Fig. 10. Molecular structure of (a) $Pt_9(CNXyl)_{13}(CO)$, (b) space filling model, (c) a simplified view of the metal skeleton and stereochemistry of the ligands, (d) metal skeleton (purple, Pt; orange, P; red, O; grey, C; blue, N; white, H). Main bond distances: Pt-Pt 2.617(2)-3.082(3)(7) Å; Pt-$C(N)_{terminal}$ 1.90(5)-1.97(5) Å; Pt-$C(N)_{bridging}$1.96(6)-2.10(5) Å; Pt-$C(O)_{bridging}$ 2.12(7)-2.13(6) Å; $C_{terminal}$-N 1.10(6)-1.19(7) Å; $C_{bridging}$-N 1.11(6)-1.21(6) Å; $C_{bridging}$-O 1.04(6) Å. For the μ_3-η^2-CNXyl: Pt-C 1.71(7), 2.06(7), 2.59(7) $C_{bridging}$-N Å; Pt-N 2.48(6) Å; C-N 1.09(8) Å.

3. Conclusions

The $[Ph_3P(CH_2)_{12}PPh_3][Pt_{18}(CO)_{36}]$ salt displays a new self-assembly mode of Chini clusters consisting of an infinite stack of $[Pt_9(CO)_{18}]^-$ units. This may be viewed as a periodic distortion of an infinite chain of $[Pt_{18}(CO)_{36}]^{2-}$ clusters which involves units of three consecutive $Pt_3(CO)_6$ triangles and not a single $Pt_3(CO)_6$ unit as previously found in symmetric and asymmetric semi-continuous arrangement of Chini clusters (Figure 1). Mono-anions of the type $[Pt_{3n}(CO)_{6n}]^-$ might be involved in the oxidation of Chini clusters [30].

The reactions of Chini clusters with isonitriles have been described here for the very first time. At difference with analogous reactions with various phosphines, Chini clusters react only with an excess of CNXyl, and the reactions proceed via redox fragmentation. Thus, the reactions of Chini clusters with soft nucleophiles strongly depend on the nature of the nucleophile. It is likely that the first step of these reactions is the addition of the nucleophile to the cluster. Then, this purported addition product may evolve via elimination of a CO ligand, leading to non-redox substitution, or via a more drastic rearrangement of the metal cage of the cluster, resulting in redox-fragmentation. To support this hypothesis, DFT calculations on the CO exchange of $[Pt_6(CO)_{12}]^{2-}$ suggest an associative interchange pathway.

After almost fifty years from their discovery, platinum carbonyl Chini clusters [1,2] still disclose new and exciting results. The mechanisms of their oxidation, reduction and substitution reactions have not yet been fully understood. This paper attempted to add a few further insights into the chemistry of these fascinating molecular clusters.

4. Experimental

4.1 General procedures.

All reactions and sample manipulations were carried out using standard Schlenk techniques under nitrogen and in dried solvents. All the reagents were commercial products (Aldrich) of the highest purity available and used as received, except $[NR_4]_2[Pt_{3n}(CO)_{6n}]$ (n = 2-6) which have been prepared according to the literature [1,2]. Analyses of C, H and N were obtained with a Thermo Quest Flash EA 1112NC instrument. IR spectra were recorded on a Perkin Elmer Spectrum One interferometer in CaF_2 cells. $^{31}P\{^1H\}$ NMR

measurements were performed on a Varian Mercury Plus 400 MHz instrument. The phosphorous chemical shifts were referenced to external H_3PO_4 (85% in D_2O). Electrical resistivity measurements have been carried out under nitrogen in a glove-bag with a Keithley 2400 Source Meter on polycrystalline materials pressed into pellets (diameter 13 mm, thickness ca. 1 mm) using the four points method. Structure drawings have been performed with SCHAKAL99 [45] and Diamond [46].

4.2 Synthesis of 1,12 bis(diphenylphosphano)dodecane, [Ph_2P-$(CH_2)_{12}$-PPh_2]

A THF solution of $KP(C_6H_5)_2$ (16.3 mL, 0.5 M in THF, 8.15 mmol) has been introduced in a Schlenk tube and cooled at -78°C. A second solution of 1,12-dichlorododecane in THF (1,01 g, 4.24 mmol in 1.5 mL) has been dropwise added to the former under stirring, getting to the precipitation of a white solid. After one hour 15 mL of water have been added and the vigorously stirred suspension. Then the organic phase has been separated, the solvent evacuated and the resulting white solid has been dissolved in toluene (35 mL) and dried with Na_2SO_4. Methanol (80 mL) has been added to the toluene solution, allowing the precipitation of the product as a white powder, filtered over Buchner and washed with methanol (yield 1.55 g, 68%).

$C_{48}H_{54}Br_2P_2$ (538.29): calcd. C 80.25, H 8.24; found: C 80.48, H 8.70. $^{31}P\{^1H\}$ NMR ($CDCl_3$, 298 K, 161.943 MHz) δ -15.6 (s) ppm.

4.3 Synthesis of 1,12-bis(triphenylphosphonium)dodecane dibromide, [Ph_3P-$(CH_2)_{12}$-PPh_3][Br_2]

In a neck glass tube, [Ph_2P-$(CH_2)_{12}$-PPh_2] (0.80, g 1.49 mmol), $NiBr_2$ (0.02 g, 0.09 mmol), bromobenzene (0.3 mL, 3.0 mmol, d= 1.49 g/mL) and ethylene glycol (1 mL) were added. The mixture was then heated at 180 °C for 4 hours. The resulting solution was then cooled down to RT and CH_2Cl_2 (20 mL) was added. The solution was put in a separating funnel and washed three times with water (30 mL). The organic phase was then dried with $MgSO_4$, filtered and concentrated by vacuum pump until the obtainment of a sticky pale yellow solid. This was redissolved in CH_2Cl_2 (5 mL) and diethylether (20 mL) was added. This resulted in the precipitation of a white solid which was filtered, washed with diethyl ether and dried by vacuum pump, finally becoming well powdered (yield 0.56 g, 44%).

$C_{48}H_{54}Br_2P_2$ (850.21): calcd. C 67.75, H 6.40; found: C 70.40, H 6.81. $^{31}P\{^1H\}$ NMR ($CDCl_3$, 298 K, 161.943 MHz) δ 25.0 (s) ppm.

4.4 Synthesis of [$Ph_3P(CH_2)_{12}PPh_3$][$Pt_{18}(CO)_{36}$]

A solution of NaOH (3.10 g, 77.5 mmol) in CH_3OH (20 mL) was added dropwise to a suspension of $Na_2[Pt_{30}(CO)_{30}]$ (1.55 g, 0.205 mmol) in CH_3OH (35 mL) and the reaction monitored by IR spectroscopy up to

the formation of a yellow-green solution of $Na_2[Pt_{15}(CO)_{30}]$. Then, a solution of $[Ph_3P(CH_2)_{12}PPh_3][Br]_2$ (0.300 g, 0.352 mmol) in H_2O (50 mL) was added and the resulting solid was recovered by filtration, washed with H_2O (3 × 20 mL), dried under reduced pressure and eventually extracted with THF (15 mL). CF_3COOH (100 μL, 1.31 mmol) was added to the resulting THF solution under CO atmosphere resulting in the immediate precipitation of a violet solid. This has been recovered by filtration, washed with THF (10 mL) and extracted with dmf (5 mL). Crystals of $[Ph_3P(CH_2)_{12}PPh_3][Pt_{18}(CO)_{36}]$ suitable for X-ray crystallography were obtained by slow diffusion of isopropanol (20 mL) on the dmf solution (yield 0.92 g, 52% based on Pt).

$C_{84}H_{54}O_{36}P_2Pt_{18}$ (5212.83): calcd. C 19.35, H 1.04; found: C 19.61, H 1.23, N 4.33. IR (dmf, 293 K) ν(CO): 2059(vs), 1902(sh), 1875(s), 1853(sh), 1840(sh) cm^{-1}.

4.5 Synthesis of $[Ph_3P(CH_2)_6PPh_3][Pt_{15}(CO)_{30}]$

A solution of NaOH (3.10 g, 77.5 mmol) in CH_3OH (20 mL) was added dropwise to a suspension of $Na_2[Pt_{30}(CO)_{30}]$ (1.55 g, 0.205 mmol) in CH_3OH (35 mL) and the reaction monitored by IR spectroscopy up to the formation of a yellow-green solution of $Na_2[Pt_{15}(CO)_{30}]$. Then, a solution of $[Ph_3P(CH_2)_6PPh_3][Br]_2$ (0.300 g, 0.819 mmol) in CH_3OH (20 mL) was added and the resulting solid was recovered by filtration, washed with CH_3OH (3 × 20 mL), acetone (20 mL) and CH_3CN (20 mL), and eventually extracted with dmf (15 mL). Crystals of $[Ph_3P(CH_2)_6PPh_3][Pt_{15}(CO)_{30}]$ suitable for X-ray crystallography were obtained by slow diffusion of isopropanol (40 mL) on the dmf solution (yield 1.11 g, 62% based on Pt).

$C_{72}H_{42}O_{30}P_2Pt_{15}$ (4375.34): calcd. C 19.76, H 0.97; found: C 19.47, H 1.18. IR (THF, 293 K) ν(CO): 2056(vs), 1896(sh), 1874(m), 1845(sh) cm^{-1}.

4.6 Synthesis of $[DAMS]_2[Pt_9(CO)_{18}]\cdot dmf$

A solution of NaOH (3.10 g, 77.5 mmol) in CH_3OH (20 mL) was added dropwise to a suspension of $Na_2[Pt_{30}(CO)_{30}]$ (1.55 g, 0.205 mmol) in CH_3OH (35 mL) and the reaction monitored by IR spectroscopy up to the formation of a red solution of $Na_2[Pt_9(CO)_{18}]$. Then, a solution of [DAMS]I (0.300 g, 0.819 mmol) in CH_3OH (20 mL) was added and the resulting solid was recovered by filtration, washed with CH_3OH (3 × 20 mL), acetone (20 mL) and CH_3CN (20 mL), and eventually extracted with dmf (15 mL). Crystals of $[DAMS]_2[Pt_9(CO)_{18}]\cdot$dmf suitable for X-ray crystallography were obtained by slow diffusion of isopropanol (40 mL) on the dmf solution (yield 0.92 g, 48% based on Pt).

$C_{53}H_{45}N_5O_{19}Pt_9$ (2811.75): calcd. C 22.63, H 1.61, N 2.49; found: C 22.31, H 1.87, N 2.16. IR (dmf, 293 K) ν(CO): 2030(vs), 1841(m) cm^{-1}.

4.7 Synthesis of $Pt_2(dppe)_3(CO)_2 \cdot 2CH_2Cl_2$

dppe (0.700 g, 2.868 mmol) was added as a solid to a solution of $[NEt_4]_2[Pt_9(CO)_{18}]$ (0.997 g, 0.396 mmol) in CH_3CN (15 mL). The resulting mixture was stirred at room temperature for 4 h affording a microcrystalline solid, which was recovered by filtration, extracted in toluene and dried under reduced pressure. The solid was extracted with CH_2Cl_2 (10 mL). Crystals of $Pt_2(dppe)_3(CO)_2 \cdot 2CH_2Cl_2$suitable for X-ray analyses were obtained by layering n-hexane (25 mL) on the CH_2Cl_2 solution (yield 0.81 g, 25 % based on Pt).

$C_{82}H_{76}Cl_4O_2P_6Pt_2$ (1811.22): calcd. C 54.42, H 4.24; found: C 54.71, H 3.87. IR (CH_2Cl_2, 293 K) ν(CO): 1913(vs) cm^{-1}.

4.8 Synthesis of $Pt_5(CNXyl)_{10} \cdot 2toluene$

Solid CNXyl (0.610 g, 4.65 mmol) was added in small portions to a CH_3CN (20 mL) solution of $[NEt_4]_2[Pt_6(CO)_{12}]$ (0.64 g, 0.362 mmol). The solution was stirred at room temperature under nitrogen for 30 minutes. Then, the solvent was removed *in vacuo*, the solid washed with water (40 mL) and extracted in toluene (15 mL). Crystals of $Pt_5(CNXyl)_{10} \cdot 2$toluene suitable for X-ray analyses were obtained by slow diffusion of n-pentane (30 mL) on the toluene solution at -20 °C (yield 0.55 g, 51% based on Pt).

$C_{104}H_{106}N_{10}Pt_5$ (2471.43): calcd. C 50.53, H 4.33, N 5.67; found: C 50.22, H 4.54, N 5.19. IR (toluene, 293 K) ν(CN): 2117(vs), 1663(m) cm^{-1}. IR (nujol mull, 293 K) ν(CN): 2111(vs), 2080(sh), 1651(s) cm^{-1}.

4.9 Synthesis of $Pt_9(CNXyl)_{13}(CO) \cdot solv$

Solid CNXyl (0.400 g, 3.05 mmol) was added in small portions to an acetone (20 mL) solution of $[NEt_4]_2[Pt_{15}(CO)_{30}]$ (0.890 g, 0.221 mmol). The solution was stirred at room temperature under nitrogen for 30 minutes. Then, the solvent was removed *in vacuo*, the solid washed with water (40mL) and extracted in toluene (15 mL). Crystals of $Pt_9(CNXyl)_{13}(CO) \cdot$solv suitable for X-ray analyses were obtained by slow diffusion of n-pentane (30 mL) on the toluene solution at -20 °C (yield 0.21 g, 16% based on Pt).

$C_{118}H_{117}N_{13}OPt_9$ (3489.05): calcd. C 40.61, H 3.38, N 5.22; found: C 40.89, H 2.97, N 4.88. IR (toluene, 293 K) ν(CN): 2112(vs), 1774(m) cm^{-1}. IR (nujol mull, 293 K) ν(CN): 2096(vs), 1770(m), 1667(s) cm^{-1}.

4.10 Synthesis of $[NEt_4]_2[Pt_{12}(CO)_{22}(PPh_2py)_2]$

Solid PPh_2py (0.206 g, 0.782 mmol) was added in small portions to an acetone (20 mL) solution of $[NEt_4]_2[Pt_{12}(CO)_{24}]$ (1.28 g, 0.391 mmol). The solution was stirred at room temperature under nitrogen for 30 minutes. Then, the solvent was removed *in vacuo*, the solid washed with water (40 mL) and toluene (40 mL), dried *in vacuo*, and extracted in acetone (20 mL). Crystals of $[NEt_4]_2[Pt_{12}(CO)_{22}(PPh_2py)_2]$ suitable for X-

ray analyses were obtained by slow diffusion of n-hexane (40 mL) on the acetone solution (yield 0.95 g, 68% based on Pt).

$C_{72}H_{68}N_4O_{22}P_2Pt_{12}$ (3744.32): calcd. C 23.09, H 1.83, N 1.50; found: C 23.33, H 2.05, N 1.21. IR (acetone, 293 K) ν(CO): 2024(vs), 1847(m) cm^{-1}. IR (nujol mull, 293 K) ν(CO): 2030(vs), 1825(m) cm^{-1}.

4.11 Synthesis of $[NEt_4]_2[Pt_9(CO)_{18}]\cdot py$

Crystals of $[NEt_4]_2[Pt_9(CO)_{18}]\cdot$py suitable for X-ray crystallography were obtained by slow diffusion of isopropanol (40 mL) on a solution of $[NEt_4]_2[Pt_9(CO)_{18}]$ (0.997 g, 0.396 mmol) in pyridine (15 mL) (yield 0.80, 78% based on Pt).

$C_{39}H_{45}N_3O_{18}Pt_9$ (2599.59): calcd. C 18.01, H 1.75, N 1.62; found: C 18.36, H 1.98, N 1.21. IR (pyridine, 293 K) ν(CO): 2031(vs), 1839(m) cm^{-1}. IR (nujol mull, 293 K) ν(CO): 2016(vs), 1811(m) cm^{-1}.

4.12 X-ray Crystallographic Study

Crystal data and collection details for $[Ph_3P(CH_2)_{12}PPh_3][Pt_{18}(CO)_{36}]$, $[Ph_3P(CH_2)_6PPh_3][Pt_{15}(CO)_{30}]$, $[DAMS]_2[Pt_9(CO)_{18}]\cdot$dmf, $Pt_2(dppe)_3(CO)_2\cdot 2CH_2Cl_2$, $Pt_5(CNXyl)_{10}\cdot$2toluene, $Pt_9(CNXyl)_{13}(CO)\cdot$solv, $[NEt_4]_2[Pt_{12}(CO)_{22}(PPh_2py)_2]$ and $[NEt_4]_2[Pt_9(CO)_{18}]\cdot$py are reported in Table 2. The diffraction experiments were carried out on a Bruker APEX II diffractometer equipped with a CCD ($[Ph_3P(CH_2)_{12}PPh_3][Pt_{18}(CO)_{36}]$, $[Ph_3P(CH_2)_6PPh_3][Pt_{15}(CO)_{30}]$, $[DAMS]_2[Pt_9(CO)_{18}]\cdot$dmf) or a PHOTON100 ($Pt_2(dppe)_3(CO)_2$, $Pt_5(CNXyl)_{10}\cdot$2toluene, $Pt_9(CNXyl)_{13}(CO)$, $[NEt_4]_2[Pt_{12}(CO)_{22}(PPh_2py)_2]$ and $[NEt_4]_2[Pt_9(CO)_{18}]\cdot$py) detector using Mo–K$\alpha$ radiation. Data were corrected for Lorentz polarization and absorption effects (empirical absorption correction SADABS) [47]. Structures were solved by direct methods and refined by full-matrix least-squares based on all data using F^2 [48]. Hydrogen atoms were fixed at calculated positions and refined by a riding model. All non-hydrogen atoms were refined with anisotropic displacement parameters, unless otherwise stated.

$[Ph_3P(CH_2)_{12}PPh_3][Pt_{18}(CO)_{36}]$: The asymmetric unit of the unit cell contains half of one cluster anion (located on a general position; the whole anion is generated by translation) and one half of a $[Ph_3P(CH_2)_{12}PPh_3]^{2+}$ cation (located on an inversion centre). The C and O-atoms of the CO ligands in the cluster anion have been restrained to isotropic behaviour (ISOR line in SHELXL, s.u. 0.01).

$[Ph_3P(CH_2)_6PPh_3][Pt_{15}(CO)_{30}]$:The asymmetric unit of the unit cell contains one half of a cluster anion (located on 2) and one half of a $[Ph_3P(CH_2)_6PPh_3]^{2+}$ cation (located on an inversion centre). The C and O-atoms have been restrained to isotropic behaviour (ISOR line in SHELXL, s.u. 0.01).

$[DAMS]_2[Pt_9(CO)_{18}]\cdot dmf$: The asymmetric unit of the unit cell contains one half of a cluster anion (located on 2), one $[DAMS]^+$ cation (located on a general position) and half of a dmf molecule disordered over two symmetry related (by m) positions. The C and O-atoms have been restrained to isotropic behaviour (ISOR line in SHELXL, s.u. 0.01). Rigid bond restraints have been applied to the cluster anion (DELU line in SHELXL, s.u. 0.01). Similar *U* restraints have been applied to the C and N atoms of the $[DAMS]^+$ cation (SIMU line in SHELXL, s.u. 0.01). The atoms of the dmf molecule have been restrained to lie on a common plane (FLAT line in SHELXL, s.u. 0.01) and to have similar *U* parameters (SIMU line in SHELXL, s.u. 0.01). Restraints to bond distances were applied as follow (s.u. 0.02): 1.21 Å for C–O, 1.37 Å for C–N and 1.46 Å for N–Me in dmf.

$Pt_2(dppe)_3(CO)_2\cdot CH_2Cl_2$: The asymmetric unit of the unit cell contains half of a platinum complex (located on an inversion centre) and one CH_2Cl_2 molecule (on a general position). Similar *U* restraints have been applied to the C atoms (SIMU line in SHELXL, s.u. 0.01).

$Pt_5(CNXyl)_{10}\cdot 2toluene$: The asymmetric unit of the unit cell contains one cluster and two toluene molecules located on general positions. Similar *U* restraints have been applied to the C and N atoms (SIMU line in SHELXL, s.u. 0.01). The C-atoms of the toluene molecules have been restrained to isotropic behaviour (ISOR line in SHELXL, s.u. 0.01) and constrained to fit regular hexagons (AFIX 66 line in SHELXL).

$Pt_9(CNXyl)_{13}(CO)\cdot solv$: The asymmetric unit of the unit cell contains one cluster molecule located on a general position. The unit cell contains an additional total potential solvent accessible void of 156 $Å^3$ (*ca*. 3% of the Cell Volume), which is likely to be occupied by highly disordered solvent molecules. These voids have been treated using the SQUEEZE routine of PLATON [49]. The C-atoms of the aromatic rings have been constrained to fit regular hexagons (AFIX 66 line in SHELXL). Similar *U* restraints have been applied to the C, O and N atoms (SIMU line in SHELXL, s.u. 0.01).

$[NEt_4]_2[Pt_{12}(CO)_{22}(PPh_2py)_2]$: The asymmetric unit of the unit cell contains half of a cluster anion (located on 2) and one $[NEt_4]^+$ cation (on a general position). Similar *U* restraints have been applied to the C, O and N atoms (SIMU line in SHELXL, s.u. 0.01). The C-atoms of the aromatic rings have been constrained to fit regular hexagons (AFIX 66 line in SHELXL). The N-atom of the PPh_2py ligand is disordered over six positions, corresponding to the *orto* positions of the three P-bonded aromatic rings. One free variable has been assigned to each position and sum of these six variables has been restrained to unit (SUMP 1.0 0.001 1.0 2 1.0 3 1.0 4 1.0 5 1.0 6 1.0 7 line in SHELXL).

$[NEt_4]_2[Pt_9(CO)_{18}]\cdot py$: The asymmetric unit of the unit cell contains one cluster anion, one $[NEt_4]^+$ cation and one pyridine molecule located on general positions, as well as two halves of two $[NEt_4]^+$ cations equally disordered over two symmetry related (by inversion centres) positions. Similar *U* restraints have been

applied to the C and N atoms of the $[NEt_4]^+$ cations and pyridine molecule (SIMU line in SHELXL, s.u. 0.01). The C and atoms of the $[NEt_4]^+$ cations have been restrained to isotropic behaviour (ISOR line in SHELXL, s.u. 0.01).

Table 2

Crystal data and experimental details for $[Ph_3P(CH_2)_{12}PPh_3][Pt_{18}(CO)_{36}]$, $[Ph_3P(CH_2)_6PPh_3][Pt_{15}(CO)_{30}]$, $[DAMS]_2[Pt_9(CO)_{18}]\cdot dmf$, $Pt_2(dppe)_3(CO)_2\cdot CH_2Cl_2$, $Pt_5(CNXyl)_{10}\cdot 2toluene$, $Pt_9(CNXyl)_{13}(CO)\cdot solv$, $[NEt_4]_2[Pt_{12}(CO)_{22}(PPh_2py)_2]$ and $[NEt_4]_2[Pt_9(CO)_{18}]\cdot py$.

	$[Ph_3P(CH_2)_{12}PPh_3]$ $[Pt_{18}(CO)_{36}]$	**$[Ph_3P(CH_2)_6PPh_3]$ $[Pt_{15}(CO)_{30}]$**	**$[DAMS]_2[Pt_9(CO)_{18}]\cdot$ dmf**
Formula	$C_{84}H_{54}O_{36}P_2Pt_{18}$	$C_{72}H_{42}O_{30}P_2Pt_{15}$	$C_{53}H_{45}N_5O_{19}Pt_9$
Fw	5212.83	4375.34	2811.75
T, K	100(2)	100(2)	298(2)
λ, Å	0.71073	0.71073	0.71073
Crystal system	Triclinic	Monoclinic	Monoclinic
Space Group	$P\bar{1}$	*C*2/*c*	*C*2/*c*
a, Å	9.417(3)	16.190(2)	20.523(8)
b, Å	15.135(5)	25.344(4)	24.368(9)
c, Å	18.573(6)	20.940(4)	14.148(5)
α, °	86.467(3)	90	90
β, °	80.733(4)	103.531(3)	113.692(4)
γ, °	75.850(3)	90	90
Cell Volume, Å^3	2532.5(13)	8354(2)	6479(4)
Z	1	4	4
D_c, g cm^{-3}	3.418	3.479	2.882
μ, mm^{-1}	24.852	25.122	19.419
F(000)	2280	7656	5008
Crystal size, mm	0.14×0.12×0.11	0.22×0.20×0.12	0.14×0.12×0.11

θ limits, °	1.388–25.027	1.523–24.999	1.368–23.533
Index ranges	-11 ≤ h ≤ 11 -18 ≤ k ≤ 18 -22 ≤ l ≤ 22	-19 ≤ h ≤ 19 -30 ≤ k ≤30 -24 ≤ l ≤ 24	-23 ≤ h ≤ 23 -27 ≤ k ≤ 27 -15 ≤ l ≤ 15
Reflections collected	22878	34045	26340
Independent reflections	8884 [R_{int} = 0.1052]	7354 [R_{int} = 0.1262]	4812 [R_{int} = 0.1347]
Completeness to θ max	99.4%	99.9%	100.0%
Data / restraints / parameters	8884 / 229 / 631	7354 / 319 / 539	4812 / 414 / 389
Goodness on fit on F^2	1.002	1.034	0.998
R_1 (I > 2σ(I))	0.0630	0.0962	0.0616
wR_2 (all data)	0.1727	0.2929	0.1831
Largest diff. peak and hole, e $Å^{-3}$	3.461 / –3.267	4.814 / –4.455	2.184 / –1.130

	$Pt_2(dppe)_3(CO)_2·2CH_2Cl_2$	**$Pt_5(CNXyl)_{10}·2toluene$**	**$Pt_9(CNXyl)_{13}(CO)·solv$**
Formula	$C_{82}H_{76}Cl_4O_2P_6Pt_2$	$C_{104}H_{106}N_{10}Pt_5$	$C_{118}H_{117}N_{13}OPt_9$
Fw	1811.22	2471.43	3489.05
T, K	100(2)	100(2)	100(2)
λ, Å	0.71073	0.71073	0.71073
Crystal system	Monoclinic	Monoclinic	Triclinic
Space Group	$P2_1/n$	$P2_1/c$	$P\bar{1}$
a, Å	15.2489(18)	22.6369(17)	14.907(3)
b, Å	12.6172(15)	14.3468(10)	15.808(3)
c, Å	20.066(3)	28.330(12)	27.254(5)

α, °	90	90	101.111(6)
β, °	102.271(4)	98.264(3)	92.914(6)
γ, °	90	90	117.372(5)
Cell Volume, Å^3	3772.5(8)	9105.2(12)	5524.3(18)
Z	2	4	2
D_c, g cm^{-3}	1.594	1.803	2.098
μ, mm^{-1}	4.020	7.708	11.401
F(000)	1796	4760	3252
Crystal size, mm	0.19×0.16×0.14	0.21×0.18×0.16	0.22×0.18×0.11
θ limits, °	1.919–25.099	1.594–26.000	1.559–25.000
Index ranges	-18 ≤ h ≤ 18 -15 ≤ k ≤ 15 -23 ≤ l ≤ 23	-27 ≤ h ≤ 27 -17 ≤ k ≤ 17 -34 ≤ l ≤ 34	-17≤ h ≤17 -18≤ k ≤18 -32≤ l ≤32
Reflections collected	40071	175320	82444
Independent reflections	6712 [R_{int} = 0.0858]	17825 [R_{int} = 0.0737]	18730 [R_{int} = 0.1218]
Completeness to θ max	100.0%	99.8%	96.2%
Data / restraints / parameters	6712 / 229 / 433	17825 / 803 / 1070	18730 / 1063 / 1175
Goodness on fit on F^2	1.166	1.240	1.265
R_1 (I > 2σ(I))	0.0551	0.0610	0.1534
wR_2 (all data)	0.1230	0.1440	0.3708
Largest diff. peak and hole, e Å^{-3}	3.245 / –2.563	2.984 / –4.145	4.960 / –6.637

	$[NEt_4]_2[Pt_{12}(CO)_{22}(PPh_2py)_2]$	$[NEt_4]_2[Pt_9(CO)_{18}]\cdot py$
Formula	$C_{72}H_{68}N_4O_{22}P_2Pt_{12}$	$C_{39}H_{45}N_3O_{18}Pt_9$
Fw	3744.32	2599.59
T, K	100(2)	100(2)
λ, Å	0.71073	0.71073
Crystal system	Monoclinic	Triclinic
Space Group	*C*2/*c*	$P\bar{1}$
a, Å	15.5558(14)	12.7967(5)
b, Å	20.2991(18)	13.1827(5)
c, Å	27.299(3)	16.4819(6)
α, °	90	94.465(2)
β, °	106.160(2)	99.793(2)
γ, °	90	109.048(2)
Cell Volume, Å^3	8279.6(14)	2563.20(17)
Z	4	2
D_c, g cm^{-3}	3.004	3.368
μ, mm^{-1}	20.295	24.526
F(000)	6680	2292
Crystal size, mm	0.22×0.18×0.16	0.19×0.16×0.13
θ limits, °	1.553–25.049	1.651–25.500
Index ranges	-18 ≤ h ≤ 18 -24≤ k ≤24 -32≤ l ≤32	-15≤ h ≤15 -15≤ k ≤ 15 -19≤ l ≤19
Reflections collected	42504	33902
Independent reflections	7271 [R_{int} = 0.0866]	9524 [R_{int} = 0.0610]
Completeness	98.9%	99.9%

to θ max		
Data / restraints / parameters	7271 / 469 / 475	9524 / 298 / 697
Goodness on fit on F^2	1.163	1.110
R_1 ($I > 2\sigma(I)$)	0.0806	0.0431
wR_2 (all data)	0.2004	0.1191
Largest diff. peak and hole, e Å^{-3}	2.638 / –2.907	3.195 / –4.140

Computational details

The ground-state geometry optimizations of $[Pt_6(CO)_{12}]^{2-}$ and $[Pt_6(CO)_{13}]^{2-}$ were carried out using the range-separated hybrid DFT functional ωB97X [50-52] in combination with Alhrichs' split-valence polarized basis set def2-SVP [53], with relativistic ECP for Pt [54]. The same theoretical approach was applied for coordinate driving calculations. The software used were Spartan 16 [55] and Gaussian 09 [56].

Appendix A. Supplementary material

CCDC 2008607-2008614 contain the supplementary crystallographic data for this paper. These data can be obtained free of charge from the Cambridge Crystallographic Data Centre.

References

[1] G. Longoni, P, Chini, J. Am. Chem. Soc. 98 (1976) 7225-7231; (b) J. C. Calabrese, L. F. Dahl, P. Chini, G. Longoni, S. Martinengo, J. Am. Chem. Soc. 96 (1974) 2614-2616.

[2] B. Berti, C. Femoni, M. C. Iapalucci, S. Ruggieri, S. Zacchini, Eur. J. Inorg. Chem. (2018) 3285-3296.

[3] I. Ciabatti, C. Femoni, M. C. Iapalucci, G. Longoni, S. Zacchini, J. Clust. Sci. 25 (2014) 115-146.

[4] C. Femoni, F. Kaswalder, M. C. Iapalucci, G. Longoni, M. Meustäbl, S. Zacchini, Chem. Commun. (2005) 5769-5771.

[5] P. Chini, G. Longoni, V. G. Albano, Adv. Organomet. Chem. 14 (1976) 285-344.

[6] D. J. Underwood, R. Hoffmann, K. Tatsumi, A. Nakamura, Y. Yamamoto, J. Am. Chem. Soc. 107 (1985) 5968-5980.

[7] (a) C. Femoni, F. Kaswalder, M. C. Iapalucci, G. Longoni, M. Meustäbl, S. Zacchini, A. Ceriotti, Angew. Chem. Int. Ed. 45 (2006) 2060-2062; (b) C. Femoni, F. Kaswalder, M. C. Iapalucci, G. Longoni, S. Zacchini, Eur. J. Inorg. Chem. (2007) 1483-1486.

[8] C. Femoni, M. C. Iapalucci, G. Longoni, T. Lovato, S. Stagni, S. Zacchini, Inorg. Chem. 49 (2010) 5992-6004.

[9] (a) P. Greco, M. Cavallini, P. Stolliar, S. D. Quiroga, S. Dutta, S. Zacchini, M. C. Iapalucci, V. Morandi, S. Milita, P. G. Merli, F. Biscarini, J. Am. Chem. Soc. 130 (2008) 1177-1182; (b) D. A. Serban, P. Greco, S. Melinte, A. Vlad, C. A. Dutu, S. Zacchini, M. C. Iapalucci, F. Biscarini, M. Cavallini, Small 5 (2009) 1117-1122.

[10] H. Remita. B. Keita, K. Torigoe, J. Belloni, L. Nadjo, Surf. Sci. 572 (2004) 301-308.

[11] M. Ichihawa in *Metal Clusters in Chemistry* (Eds.: P. Braunstein, L. A. Oro, P. R. Raithby), Wiley-VCH, New York (1999) 1273-1301.

[12] (a) S. Bhaduri, Curr. Sci. 78 (2000) 1318-1324; (b) N. S. Gupta, S. Basu, P. Payara, P. Mathur, S. Bhaduri, G. K. Lahiri, Dalton Trans. (2007) 2594-2598.

[13] D. Bonincontro, A. Lolli, A. Storione, A. Gasparotto, B. Berti, S. Zacchini, N. Dimitratos, S. Albonetti, Appl. Catal. A 588 (2019) 117279.

[14] (a) A. Fukuoka, N. Higashimoto, Y. Sakamoto, M. Sasaki, N. Sugimoto, S. Inagaki, Y. Fukushima, M. Ichikawa, Catal. Today 66 (2001) 23-28; (b) F. A. Henglein, J. Phys. Chem. B 101 (1997) 5889-5894.

[15] (a) P. Maity, S. Basu, S. Bhaduri, G. K. Lahiri, Adv. Synth. Catal. 349 (2007) 1955-1962; (b) P. Maity, C. S. Gopinath, S. Bhaduri, G. K. Lahiri, Green Chem. 11 (2009) 554-561; (c) P. Maity, S. Basu, S. Bhaduri, G. K. Lahiri, J. Mol. Catal. A 270 (2007) 117-122.

[16] (a) E. Kowalaska, H. Remita, C. Colbeau-Justin, J. Hupka, J. Belloni, J. Phys. Chem. C 112 (2008) 1124-1231; (b) G. Chen, H. Yang, B. Wu, Y. Sheng, N. Zheng, Dalton Trans. 42 (2013) 12699-12705.

[17] (a) J.-R. Chang, D. C. Koninsberger, B. C. Gates, J. Am. Chem. Soc. 114 (1992) 6460-6466; (b) L. Drozdová, L. Brabec, J. Nováková, M. Beneke, N. I. Jaeger, G. Schulz-Ekloff, Microporous Mesoporous Mater. 35-36 (2000) 511-519.

[18] V. Sebastian, C. D. Smith, K. F. Jensen, Nanoscale 8 (2016) 7534-7543.

[19] (a) G. J. Lewis, J. D. Roth, R. A. Montag, L. K. Safford, X. Gao, S.-C. Chang, L. F. Dahl, M. J. Weaver, J. Am. Chem. Soc. 112 (1990) 2831-2832; (b) J. D. Roth, G. J. Lewis, L. K. Safford, X. Jiang, L. F. Dahl, M. J. Weaver, J. Am. Chem. Soc. 114 (1992) 6159-5169.

[20] I. B. Arago, J. M. C. Bueno, D. Zanchet, Appl. Catal. A 568 (2018) 86-94.

[21] K. Kratzl, T. Kratky, S. Günther, O. Tomanec, R. Zbořil, J. Michalička, J. M. Macak, M. Cokoja, R. A. Fischer, J. Am. Chem. Soc. 35 (2019) 13962-13969.

[22] (a) L. K. Batchelor, B. Berti, C. Cesari, I. Ciabatti, P. J. Dyson, C. Femoni, M. C. Iapalucci, M. Mor, S. Ruggieri, S. Zacchini, Dalton Trans. 47 (2018) 4467-4477; (b) I. Ciabatti, C. Femoni, M. C. Iapalucci, G. Longoni, T. Lovato, S. Zacchini, Inorg. Chem. 52 (2013) 4384-4395; (c) I. Ciabatti, C. Femoni, M. C. Iapalucci, G. Longoni, S. Zacchini, Organometallics 32 (2013) 5180-5189.

[23] B. Berti, C. Cesari, F. Conte, I. Ciabatti, C. Femoni, M. C. Iapalucci, F. Vacca, S. Zacchini, Inorg. Chem. 57 (2018) 7578-7590.

[24] C. Cesari, I. Ciabatti, C. Femoni, M. C. Iapalucci, F. Mancini, S. Zacchini, Inorg. Chem. 56 (2017) 1665-1668.

[25] (a) E. Cattabriga, I. Ciabatti, C. Femoni, M. C. Iapalucci, G. Longoni, S. Zacchini, Inorg. Chim. Acta 470 (2018) 238-249; (b) E. Cattabriga, I. Ciabatti, C. Femoni, T. Funaioli, M. C. Iapalucci, S. Zacchini, Inorg. Chem. 55 (2016) 6068-6079.

[26] M. Bortoluzzi, C. Cesari, I. Ciabatti, C. Femoni, M. C. Iapalucci, S. Zacchini, Inorg. Chem. 56 (2017) 6532-6544.

[27] (a) I. Ciabatti, C. Femoni, M. C. Iapalucci, G. Longoni, S. Zacchini, S. Zarra, Nanoscale 4 (2012) 4166-4177; (b) C. Femoni, M. C. Iapalucci, G. Longoni, S. Zacchini, S. Zarra, J. Am. Chem. Soc. 133 (2011) 2406-2409.

[28] B. Berti, M. Bortoluzzi, C. Cesari, C. Femoni, M. C. Iapalucci, S. Zacchini, Inorg. Chim. Acta 503 (2020) 119432.

[29] (a) M. Bortoluzzi, A. Ceriotti, I. Ciabatti, R. Della Pergola, C. Femoni, M. C. Iapalucci, A. Storione, S. Zacchini, Dalton Trans. 45 (2016) 5001-2013; (b) M. Bortoluzzi, A. Ceriotti, C. Cesari, I. Ciabatti, R. Della Pergola, C. Femoni, M. C. Iapalucci, A. Storione, S. Zacchini, Eur. J. Inorg. Chem. (2016) 3939-3949.

[30] P. Archirel, J. Phys. Chem. C 120 (2016) 8343-8353.

[31] R. G. Peters, B. L. Bennett, D. M. Roddick, Inorg. Chim. Acta 265 (1997) 205-211.

[32] (a) V. G. Albano, P. Bellon, M. Sansoni, J. Chem. Soc. A (1971) 2420-2425; (b) V. G. Albano, G. M. B. Ricci, P. Bellon, Inorg. Chem. 8 (1969) 2109-2115.

[33] (a) C. Brown, B. T. Heaton, P. Chini, A. Fumagalli, G. Longoni, J. Chem. Soc., Chem. Commun. (1977) 309-311; (b) C. Brown, B. T. Heaton, A. D. C. Towl, P. Chini, A. Fumagalli, G. Longoni, J. Organomet. Chem. 181 (1979) 233-254.

[34] B. R. Barnett, A. L. Rheingold, J. S. Figueroa, Angew. Chem. Int. Ed. 55 (2016) 9253-9258.

[35] (a) J.-P. Barbier, R. Bender, P. Braunstein, J. Fischer, L. Ricard, J. Chem. Res. 230 (1978) 2913-2918; (b) Z. Beni, R. Ros, A. Tassan, R. Scopelliti, R. Roulet, Inorg. Chim. Acta 358 (2005) 497-503; (c) J. B. Ballif, P. Braunstein, A. D. Burrows, R. D. Adams, W. Wu, J. Cluster Sci. 5 (1994) 443-466.

[36] (a) D. M. P. Mingos, D. J. Wales, Introduction to Cluster Chemistry, Prentice Hall, Englewood Cliffs (1990); (b) J.-F. Halet, D. G. Evans, D. M. P. Mingos, J. Am. Chem. Soc. 110 (1988) 87-90; (c) K. Wade, Adv. Inorg. Chem. Radiochem. 18 (1976) 1-66.

[37] M. Schulz-Dobrick, M. Jansen, Angew. Chem. Int. Ed. 47 (2008) 2256-2259.

[38] (a) J. A. Cabeza, I. del Río, P. García-Álvarez, D. Miguel, Organometallics 25 (2006) 5672-5675; (b) D. A. Krogstad, V. G. Young Jr, L. H. Pignolet, Inorg. Chim. Acta 264 (1997) 19-32.

[39] M. Ohashi, J. Yi, D. Shimizu, T. Yamagata, T. Ohshima, K. Mashima, J. Organomet. Chem. 691 (2006) 2457-2464.

[40] O. Shawkataly, S.-G. Teoh, H.-K. Fun, J. Organomet. Chem. 464 (1994) C29-C30.

[41] Y. Yamamoto, K. Aoki, H. Yamazaki, Organometallics2 (1983) 1377-1381.

[42] V. W. Day, R. O. Day, J. S. Kristoff, F. J. Hirsekorn, E. L. Muetterties, J. Am. Chem. Soc. 97 (1975) 2571-2573.

[43] C. R. Eady, P. D. Gavens, B. F. G. Johnson, J. Lewis, M. C. Malatesta, M. J. Mays, A. G. Orpen, A. V. Rivera, G. M. Sheldrick, M. B. Hursthouse, J. Organomet. Chem. 149 (1978) C43-C46.

[44] O. J. Scherer, R. Walter, W. S. Sheldrick, Angew. Chem. Int. Ed. 24 (1985) 115-117.

[45] E. Keller, SCHAKAL99, University of Freiburg, Germany, 1999.

[46] DIAMOND - Visual Crystal Structure Information System, CRYSTAL IMPACT, Postfach 1251, D-53002 Bonn.

[47] G. M. Sheldrick, SADABS-2008/1 - Bruker AXS Area Detector Scaling and Absorption Correction, Bruker AXS, Madison, Wisconsin, USA, 2008.

[48] G. M. Sheldrick, Acta Crystallogr. C71 (2015) 3-8.

[49] (a) A. L. Spek, J. Appl. Cryst. 36 (2003) 7-13; (b) A. L. Spek, Acta Cryst. D65 (2009) 148-155.

[50] Y. Minenkov, Å. Singstad, G. Occhipinti, V. R. Jensen, Dalton Trans. 41 (2012) 5526-5541.

[51] J.-D. Chai, M. Head-Gordon, Phys. Chem. Chem. Phys. 10 (2008) 6615-6620.

[52] I. C. Gerber, J. G. Ángyán, Chem. Phys. Lett. 415 (2005) 100-105.

[53] F. Weigend, R. Ahlrichs, Phys. Chem. Chem. Phys. 7 (2005) 3297-3305.

[54] D. Andrae, U. Häußermann, M. Dolg, H. Stoll, H. Preuß, Theor. Chim. Acta 77 (1990) 123-141.

[55] (a) Spartan'16, Build 2.0.3, Wavefunction Inc., Irvine CA, USA, 2016. (b) Y. Shao, Z. Gan, E. Epifanovsky, A. T. B. Gilbert, M. Wormit, J. Kussmann, A. W. Lange, A. Behn, J. Deng, X. Feng, D. Ghosh, M. Goldey, P. R. Horn, L. D. Jacobson, I. Kaliman, R. Z. Khaliullin, T. Kus', A. Landau, J. Liu, E. I. Proynov, Y. M. Rhee, R. M. Richard, M. A. Rohrdanz, R. P. Steele, E. J. Sundstrom, H. L. Woodcock III, P. M. Zimmerman, D. Zuev, B. Albrecht, E. Alguire, B. Austin, G. J. O. Beran, Y. A. Bernard, E. Berquist, K. Brandhorst, K. B. Bravaya, S. T. Brown, D. Casanova, C.-M. Chang, Y. Chen, S. H. Chien, K. D. Closser, D. L. Crittenden, M. Diedenhofen, R. A. Di Stasio Jr., H. Do, A. D. Dutoi, R. G. Edgar, S. Fatehi, L. Fusti-Molnar, A. Ghysels, A. Golubeva-Zadorozhnaya, J. Gomes, M. W. D. Hanson-Heine, P. H. P. Harbach, A. W. Hauser, E. G. Hohenstein, Z. C. Holden, T.-C. Jagau, H. Ji, B. Kaduk, K. Khistyaev, J. Kim, J. Kim, R. A. King, P. Klunzinger, D. Kosenkov, T. Kowalczyk, C. M. Krauter, K. U. Lao, A. D. Laurent, K. V. Lawler, S. V. Levchenko, C. Y. Lin, F. Liu, E. Livshits, R. C. Lochan, A. Luenser, P. Manohar, S. F. Manzer, S.-P. Mao, N. Mardirossian, A. V. Marenich, S. A. Maurer, N. J. Mayhall, E. Neuscamman, C. Melania Oana, R. Olivares-Amaya, D. P. O'Neill, J. A. Parkhill, T. M. Perrine, R. Peverati, A. Prociuk, D. R. Rehn, E. Rosta, N. J. Russ, S. M. Sharada, S. Sharma, D. W. Small, A. Sodt, T. Stein, D. Stück, Y.-C. Su, A. J. W. Thom, T. Tsuchimochi, V. Vanovschi, L. Vogt, O. Vydrov, T. Wang, M. A. Watson, J. Wenzel, A. White, C. F. Williams, J. Yang, S. Yeganeh, S. R. Yost, Z.-Q. You, I. Y. Zhang, X. Zhang, Y. Zhao, B. R. Brooks, G. K. L. Chan, D. M. Chipman, C. J. Cramer, W. A. Goddard III, M. S. Gordon,

W. J. Hehre, A. Klamt, H. F. Schaefer III, M. W. Schmidt, C. David Sherrill, D. G. Truhlar, A. Warshel, X. Xu, A. Aspuru-Guzik, R. Baer, A. T. Bell, N. A. Besley, J.-D. Chai, A. Dreuw, B. D. Dunietz, T. R. Furlani, S. R. Gwaltney, C.-P. Hsu, Y. Jung, J. Kong, D. S. Lambrecht, W. Liang, C. Ochsenfeld, V. A. Rassolov, L. V. Slipchenko, J. E. Subotnik, T. Van Voorhis, J. M. Herbert, A. I. Krylov, P. M. W. Gill, M. Head-Gordon, Mol. Phys. 113 (2015) 184-215.

[56] M. J. Frisch, G. W. Trucks, H. B. Schlegel, G. E. Scuseria, M. A. Robb, J. R. Cheeseman, G. Scalmani, V. Barone, B. Mennucci, G. A. Petersson, H. Nakatsuji, M. Caricato, X. Li, H. P. Hratchian, A. F. Izmaylov, J. Bloino, G. Zheng, J. L. Sonnenberg, M. Hada, M. Ehara, K. Toyota, R. Fukuda, J. Hasegawa, M. Ishida, T. Nakajima, Y. Honda, O. Kitao, H. Nakai, T. Vreven, J. A. Montgomery Jr., J. E. Peralta, F. Ogliaro, M. Bearpark, J. J. Heyd, E. Brothers, K. N. Kudin, V. N. Staroverov, R. Kobayashi, J. Normand, K. Raghavachari, A. Rendell, J. C. Burant, S. S. Iyengar, J. Tomasi, M. Cossi, N. Rega, J. M. Millam, M. Klene, J. E. Knox, J. B. Cross, V. Bakken, C. Adamo, J. Jaramillo, R. Gomperts, R. E. Stratmann, O. Yazyev, A. J. Austin, R. Cammi, C. Pomelli, J. W. Ochterski, R. L. Martin, K. Morokuma, V. G. Zakrzewski, G. A. Voth, P. Salvador, J. J. Dannenberg, S. Dapprich, A. D. Daniels, Ö. Farkas, J. B. Foresman, J. V. Ortiz, J. Cioslowski and D. J. Fox, Gaussian 09, Revision C.01, Gaussian Inc., Wallingford, CT, 2010.